Received: 14 March 2024 | Revised: 28 August 2024 | Accepted: 8 September 2024

DOI: 10.1002/met.70001

Meteorological Applications
Science and Technology for Weather and Climate
Open Access
RMetS

RESEARCH ARTICLE

High-resolution CMIP6 analysis highlights emerging climate challenges in alpine and Tibetan Tundra zones

Bijan Fallah[1,2] | **Masoud Rostami**[1,3] | **Iulii Didovets**[1] | **Zhiwen Dong**[4]

[1]Potsdam Institute for Climate Impact Research (PIK), Potsdam, Germany

[2]German Climate Computing Center DKRZ, Hamburg, Germany

[3]Laboratoire de Météorologie Dynamique (LMD), Sorbonne University (SU), Ecole Normale Supérieure (ENS), Paris, France

[4]State Key Laboratory of Cryosphere Sciences, Northwest Institute of Eco-Environment and Resources, Chinese Academy of Sciences, Lanzhou, China

Correspondence
Bijan Fallah, Potsdam Institute for Climate Impact Research (PIK), P.O. Box 60 12 03, Potsdam, Brandenburg 14412, Germany.
Email: fallah@pik-potsdam.de

Funding information
Virgin Unite USA, Inc; German Federal Foreign Office

Abstract

We employ a high-resolution Köppen climate classification dataset to examine shifts in Tundra zones within the Alps and Asia. Our analysis shows substantial reductions in Tundra areas by the mid-21st century under different Shared. Socioeconomic pathways (SSP1-2.6, SSP3-7.0, SSP5-8.5). Tundra zones in the Alps and the Tibetan Plateau are crucial for their unique climates and role as water reservoirs. Characterized by short, mild summers and long, severe winters, these zones are vital for the glaciers and perennial snow. The projected climate instability may significantly reduce alpine snow cover by mid-century with irreversible consequences. A 2°C temperature increase from the 1981–2010 baseline could eliminate the Tundra climate in the Alps and reduce it by over 70% in Asia. This is particularly concerning given that rivers from the Tibetan Plateau sustain nearly 40% of the global population.

KEYWORDS

Alps, Asia, *climate change*, Europe, Köppen classification, Tibetan plateau, Tundra

1 | INTRODUCTION

Policy-makers require high-resolution climate datasets for creating effective local adaptation strategies (Flato et al., 2014). Detailed climate data strengthen cross-sectoral impact assessments by enabling researchers to consider the complex interactions between climate variables and socioeconomic factors (Dunford, Smith, et al., 2015; Jäger et al., 2015). For instance, in agriculture, high-resolution data support models that forecast changes in crop viability and water resource availability under different climate scenarios (Brown et al., 2015; Dunford, Smith, et al., 2015; Holman & Cojocaru, 2011). Climate change indicators, such as the Köppen climate classification (Geiger et al., 2012; Peel et al., 2007), are essential tools for climate impact studies, especially in regions with complex topography (Brown et al., 2015; Dunford, Harrison, & Rounsevell, 2015; Fallah et al., 2023). The Köppen system categorizes the climate zones based on temperature and precipitation.

Applying the high-resolution Köppen system helps to identify slight but meaningful shifts in climate zones (Beck et al., 2018). The Tundra zone is characterized by a cold environment and short growing seasons, which are vulnerable to warming. The Tundra is an essential carbon reservoir. Warming temperatures threaten to transform these areas into carbon sources and accelerate climate change.

In this study, we use the 1-km Köppen dataset from the Climatologies at High Resolution for the Earth's Land Surface Areas (CHELSA) (Karger et al., 2017, 2020, 2021). These high-resolution data are essential for impact

modeling, providing an ecologically meaningful classification of climate zones, which is vital for assessing biodiversity responses to climate change (Brown et al., 2015; Holman & Cojocaru, 2011; Kebede et al., 2015).

These data provide an ecologically meaningful classification of climate zones for assessing biodiversity changes due to climate change (Brown et al., 2015; Holman & Cojocaru, 2011; Kebede et al., 2015). Our analysis focuses on the Alps and the Tibetan Plateau, particularly emphasizing the Tundra climate zone. The Tibetan Plateau, which is warming faster than the global average, is a critical water source for major rivers such as the Yangtze, Yellow, Mekong, and Indus (Clima & Te, 2023). The Tibetan Plateau is among the essential drivers of the atmospheric dynamics in the Northern Hemisphere, affecting monsoon systems and weather patterns across Asia (Fallah et al., 2016; Song et al., 2010). Melting glaciers jeopardize water supplies and increase the risk of floods. As permafrost thaws, greenhouse gases are released, further intensifying global warming and destabilizing landscapes.

The Alps are critical for rivers like the Rhine, Rhone, and Po. Understanding how Tundra zones are likely to shift allows for better management of natural resources, protection of ecosystems, and preparation of communities for future scenarios.

We address the following scientific questions:

- Q1: Which climates might replace the Tundra climate zones in the Alps and Asia in the future?
- Q2: What are the projected impacts of surpassing a 2°C temperature increase on the geographical distribution of the Tundra climate zone?

2 | DATA AND METHODS

2.1 | Shared socioeconomic pathways

The Shared Socioeconomic Pathways (SSPs) are scenarios developed to study the potential impacts of climate change under different socioeconomic conditions. These scenarios are utilized with Representative Concentration Pathways (RCPs), which describe different trajectories for greenhouse gas concentrations. The Intergovernmental Panel on Climate Change's (IPCC) Sixth Assessment Report (AR6) extensively reviews literature using SSP scenarios' outcomes (Eyring et al., 2016; O'neill et al., 2016).

Here, we present a summary of the SSPs used in this study:

- SSP1-2.6: Represents a sustainable development scenario that maintains global warming below 2°C. This scenario requires strong climate policies and mitigation of greenhouse gases.
- SSP3-7.0: Depicts a world characterized by regional conflicts, slow economic growth, and moderate to high greenhouse gas emissions.
- SSP5-8.5: Represents a scenario with rapid economic growth dependent on fossil energy, leading to maximum greenhouse gas emissions and significant global warming.

TABLE 1 Details of the CMIP6 models used in the study.

Model	Resolution	Components
GFDL-ESM4	Atmosphere: 1° × 1° Ocean: 1° × 1°	Atmosphere: FV3 Ocean: MOM6 Land: LM4.1
IPSL-CM6A-LR	Atmosphere: 2° × 2° Ocean: 1° × 1°	Atmosphere: LMDZ6 Ocean: NEMO v3.6 Land: ORCHIDEE
MPI-ESM1-2-HR	Atmosphere: 1° × 1° Ocean: 0.4° × 0.4°	Atmosphere: ECHAM6.3 Ocean: MPIOM Land: JSBACH
MRI-ESM2-0	Atmosphere: 1° × 1° Ocean: 1° × 1°	Atmosphere: GSM4 Ocean: COCO4.9 Land: MRI land model
UKESM1-0-LL	Atmosphere: 1.25° × 1.875° Ocean: 1° × 1°	Atmosphere: HadGEM3-GC3.1 Ocean: MEDUSA Land: JULES

We use the datasets base on five Coupled Model Intercomparison Project Phase 6 (CMIP6) models, identified as "priority" within the Inter-Sectoral Impact Model Intercomparison Project phase 3b (ISIMIP3b): GFDL-ESM4, IPSL-CM6A-LR, MPI-ESM1-2-HR, MRI-ESM2-0, and UKESM1-0-LL (Lange, 2019). Three models have low climate sensitivity, and two have high sensitivity, ensuring a balanced representation of the CMIP6 ensemble. Furthermore, these models were selected due to their structural independence in ocean and atmosphere components. Their process representations were considered reliable by climate impact modelers (Lange, 2021). Additionally, their selection aligns with previous ISIMIP phases, maintaining consistency and comparability with previous studies. Table 1 presents the descriptions of the CMIP6 models used in the study.

The ISIMIP3b bias adjustment process utilizes statistical downscaling and bias adjustment techniques to make model outputs like the observed ones. The bias adjustment and statistical downscaling codes of ISIMIP3BASD and W5E5 (Water and Global Change Forcing Data for the 5th version, v2.0) are employed to produce climate

projection input data for CHELSA (Lange et al., 2021). We consider uncertainty using the range of projections produced by different models and scenarios (SSP1-2.6, SSP2-4.5, and SSP5-8.5).

2.2 | CHELSA climatologies for historical period

The foundational data for CHELSA climatologies were derived from the European Centre for Medium-Range Weather Forecasts (ECMWF) Reanalysis Interim (ERA-Interim) reanalysis (Dee et al., 2011), which provides large-scale atmospheric variables at a coarse resolution of approximately 0.75° latitude/longitude. The downscaling process involved statistically adjusting these coarse-scale outputs to a finer spatial resolution of 30 arc seconds (~1 km^2). This enables impact modelers to study the small-scale topographic and climatic variations essential for ecological and environmental applications.

The downscaling of temperatures utilized the vertical temperature gradients (lapse rates) from the ERA-Interim data, which were corrected for elevation using a digital elevation model (DEM). The lapse rates were interpolated to sea level and re-projected onto the terrain using the DEM. This allows for accurate temperature representation across complex terrains (Karger et al., 2017).

For precipitation, the downscaling incorporated orographic predictors such as wind fields, valley exposition, and boundary layer height to refine the precipitation distribution. The resulting precipitation fields were further bias-corrected using gauge-derived products from the Global Precipitation Climatology Centre (GPCC) (Schneider et al., 2014) and the Global Historical Climatology Network (GHCN) (Lawrimore et al., 2011).

2.3 | CHELSA climatologies for future scenarios

The CHELSA climatologies for future scenarios apply similar downscaling and bias correction methodologies used for the historical climatologies but are specifically adapted to future climate model outputs. The raw outputs from the CMIP6 models, which typically have coarser resolutions (around 1° or more), are downscaled to a finer resolution (30 arc seconds) using statistical downscaling methods similar to those used for historical data. As with historical data, bias correction is applied to the downscaled CMIP6 projections. This process involves comparing the model outputs to observed data, such as those from the GHCN, or high-resolution reanalysis data like ECMWF Reanalysis 5th Generation (ERA5). This comparison is used to correct systematic biases in the climate model outputs.

After downscaling and bias correction, monthly climatologies for future periods (e.g., 2021–2040, 2041–2060, and 2061–2100) are generated. These climatologies provide high-resolution projections of future climate under different SSP scenarios.

2.4 | Validation of CHELSA climatologies

Karger et al. (2017) show that validating historical climatologies involves multiple steps. First, a cross-validation approach is employed on the meteorological station data, where 20% of stations are randomly omitted, and the remaining 80% are used for bias correction. This process is repeated multiple times, showing that the bias correction significantly improves the accuracy of the precipitation and temperature estimates. The final climatological products are compared against other gridded products and independent meteorological station data. They conclude that CHELSA's predictions are comparable to or even better than other high-resolution climate datasets, particularly in complex terrains.

The models used in these scenarios are often validated against historical climate data using a process known as hindcasting. Historical inputs drive the models, and their outputs are compared with observations. This comparison helps identify and correct biases in the models. The iterative refinement of these models ensures that they better capture the vital climatic processes and increases the reliability of their future projections. However, it is essential to acknowledge that uncertainties remain in future climate projections, and these uncertainties must be carefully considered.

2.5 | Köppen-Geiger climate classification

The Köppen-Geiger climate classification dataset was constructed by applying the Köppen-Geiger classification algorithm to high-resolution temperature and precipitation data derived from the CHELSA climatologies, thereby categorizing global climates based on these key climatic variables.

For our analysis, we utilized the 'kg02' variable from the CHELSA bioclim dataset, a high-resolution set of climatological information tailored for ecological applications. This layer represents the Köppen-Geiger climate

TABLE 2 Köppen Climate Classification Mapping. The variables used are as follows: T_m: Mean monthly temperature (in degrees Celsius). T_a: Mean annual temperature (in degrees Celsius). P_a: Annual precipitation (in millimeters). P_s: Precipitation of the wettest month (in millimeters). P_w: Precipitation of the driest month (in millimeters). P_d: Precipitation of the driest month in summer (in millimeters). T_{hmax}: Temperature of the hottest month (in degrees Celsius). T_{mmax}: Temperature of the warmest month (in degrees Celsius). T_{mmin}: Temperature of the coldest month (in degrees Celsius). P_t: Threshold precipitation, calculated as $P_t = 2 \cdot T_a + 14$ for coastal areas and $P_t = 2 \cdot T_a$ for continental areas.

Code	Climate classification	Metrics
1	Af—Equatorial fully humid	$T_m \geq 18^\circ\text{C}, P_a \geq 60\,\text{mm}$
2	Am—Equatorial monsoonal	$T_m \geq 18^\circ\text{C}, 1000 \geq P_a \geq 60\,\text{mm}$
3	As—Equatorial summer dry	$T_m \geq 18^\circ\text{C}, P_s < P_w$
4	Aw—Equatorial winter dry	$T_m \geq 18^\circ\text{C}, P_w < P_s$
5	BWk—Cold desert	$T_a < 18^\circ\text{C}, P_a < 10 \cdot P_t$
6	BWh—Hot desert	$T_a \geq 18^\circ\text{C}, P_a < 10 \cdot P_t$
7	BSk—Cold steppe	$T_a < 18^\circ\text{C}, P_a \geq 10 \cdot P_t$
8	BSh—Hot steppe	$T_a \geq 18^\circ\text{C}, P_a \geq 10 \cdot P_t$
9	Cfa—Warm temperate fully humid hot summer	$-3^\circ\text{C} < T_m < 18^\circ\text{C}, T_{hmax} \geq 22^\circ\text{C}, P_s \geq 30\,\text{mm}$
10	Cfb—Warm temperate fully humid warm summer	$-3^\circ\text{C} < T_m < 18^\circ\text{C}, 10^\circ\text{C} < T_{hmax} < 22^\circ\text{C}, P_s \geq 30\,\text{mm}$
11	Cfc—Warm temperate fully humid cool summer	$-3^\circ\text{C} < T_m < 18^\circ\text{C}, T_{hmax} \leq 10^\circ\text{C}, P_s \geq 30\,\text{mm}$
12	Csa—Warm temperate summer dry hot summer	$-3^\circ\text{C} < T_m < 18^\circ\text{C}, T_{hmax} \geq 22^\circ\text{C}, P_d < 30\,\text{mm}$
13	Csb—Warm temperate summer dry warm summer	$-3^\circ\text{C} < T_m < 18^\circ\text{C}, 10^\circ\text{C} < T_{hmax} < 22^\circ\text{C}, P_d < 30\,\text{mm}$
14	Csc—Warm temperate summer dry cool summer	$-3^\circ\text{C} < T_m < 18^\circ\text{C}, T_{hmax} \leq 10^\circ\text{C}, P_d < 30\,\text{mm}$
15	Cwa—Warm temperate winter dry hot summer	$-3^\circ\text{C} < T_m < 18^\circ\text{C}, T_{hmax} \geq 22^\circ\text{C}, P_w < P_s$
16	Cwb—Warm temperate winter dry warm summer	$-3^\circ\text{C} < T_m < 18^\circ\text{C}, 10^\circ\text{C} < T_{hmax} < 22^\circ\text{C}, P_w < P_s$
17	Cwc—Warm temperate winter dry cool summer	$-3^\circ\text{C} < T_m < 18^\circ\text{C}, T_{hmax} \leq 10^\circ\text{C}, P_w < P_s$
18	Dfa—Snow fully humid hot summer	$T_m \leq -3^\circ\text{C}, T_{hmax} \geq 22^\circ\text{C}, P_s \geq 30\,\text{mm}$
19	Dfb—Snow fully humid warm summer	$T_m \leq -3^\circ\text{C}, 10^\circ\text{C} < T_{hmax} < 22^\circ\text{C}, P_s \geq 30\,\text{mm}$
20	Dfc—Snow fully humid cool summer	$T_m \leq -3^\circ\text{C}, T_{hmax} \leq 10^\circ\text{C}, P_s \geq 30\,\text{mm}$
21	Dfd—Snow fully humid extremely continental	$T_m \leq -3^\circ\text{C}, T_{hmax} \leq 10^\circ\text{C}, P_s \geq 30\,\text{mm}, T_{mmin} < -38^\circ\text{C}$
22	Dsa—Snow summer dry hot summer	$T_m \leq -3^\circ\text{C}, T_{hmax} \geq 22^\circ\text{C}, P_d < 30\,\text{mm}$
23	Dsb—Snow summer dry warm summer	$T_m \leq -3^\circ\text{C}, 10^\circ\text{C} < T_{hmax} < 22^\circ\text{C}, P_d < 30\,\text{mm}$
24	Dsc—Snow summer dry cool summer	$T_m \leq -3^\circ\text{C}, T_{hmax} \leq 10^\circ\text{C}, P_d < 30\,\text{mm}$
25	Dsd—Snow summer dry extremely continental	$T_m \leq -3^\circ\text{C}, T_{hmax} \leq 10^\circ\text{C}, P_d < 30\,\text{mm}, T_{mmin} < -38^\circ\text{C}$
26	Dwa—Snow winter dry hot summer	$T_m \leq -3^\circ\text{C}, T_{hmax} \geq 22^\circ\text{C}, P_w < P_s$
27	Dwb—Snow winter dry warm summer	$T_m \leq -3^\circ\text{C}, 10^\circ\text{C} < T_{hmax} < 22^\circ\text{C}, P_w < P_s$
28	Dwc—Snow winter dry cool summer	$T_m \leq -3^\circ\text{C}, T_{hmax} \leq 10^\circ\text{C}, P_w < P_s$
29	Dwd—Snow winter dry extremely continental	$T_m \leq -3^\circ\text{C}, T_{hmax} \leq 10^\circ\text{C}, P_w < P_s, T_{mmin} < -38^\circ\text{C}$
30	ET—Polar Tundra	$T_{mmax} < 10^\circ\text{C}, T_{mmin} \geq 0^\circ\text{C}$
31	EF—Polar frost	$T_{mmax} < 0^\circ\text{C}$

classification and draws on the updated global climate zones map by Peel et al. (2007). The explanation of the matrices used is listed in Table 2, and the variables applied are as follows:

- T_m: Mean monthly temperature (in degrees Celsius).
- T_a: Mean annual temperature (in degrees Celsius).
- P_a: Annual precipitation (in millimeters).
- P_s: Precipitation of the wettest month (in millimeters).
- P_w: Precipitation of the driest month (in millimeters).
- P_d: Precipitation of the driest month in summer (in millimeters).

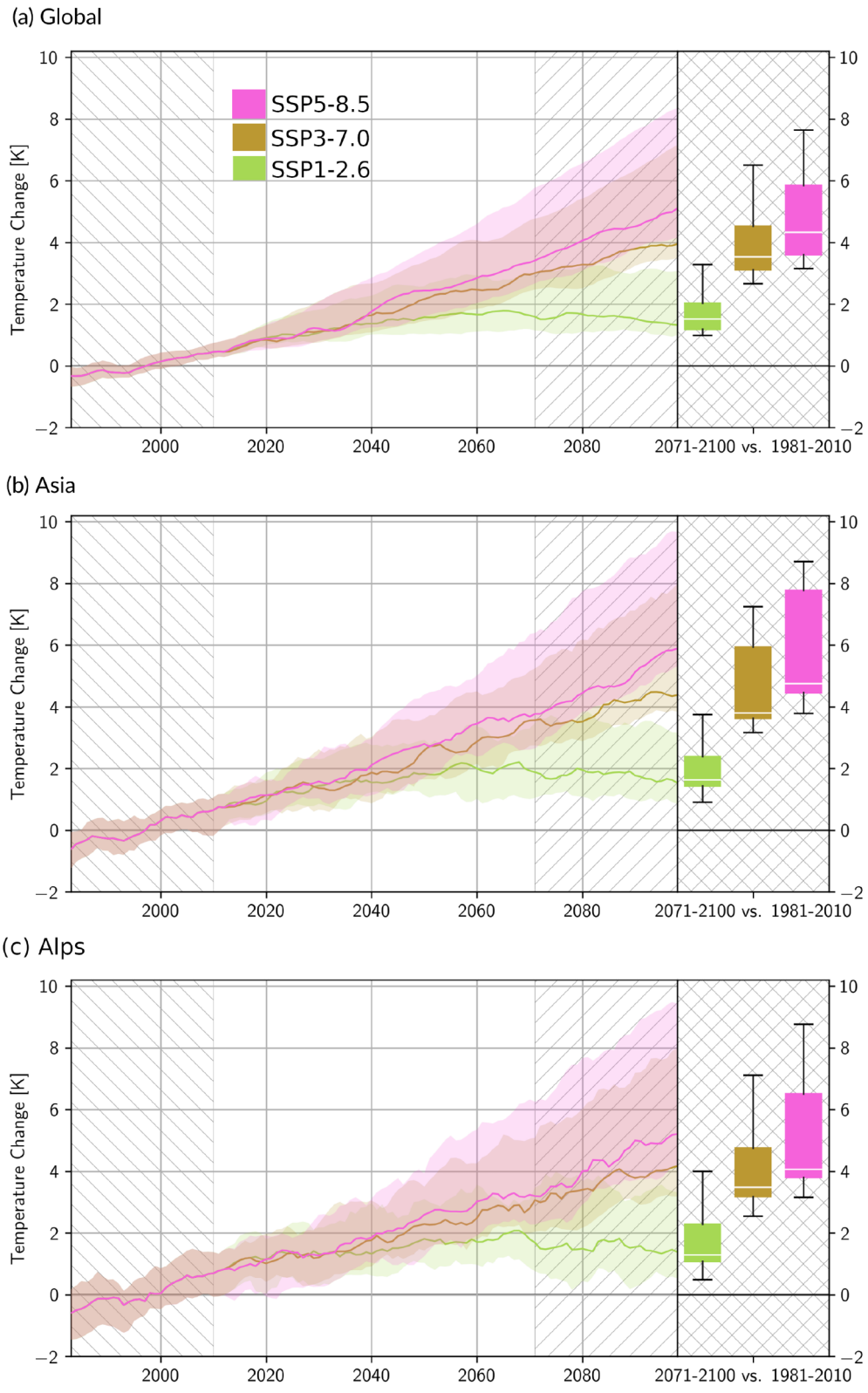

FIGURE 1 Warming trend (near-surface air temperature anomalies with respect to 1981–2010) from ISIMIP3b "priority" models for (a) global, (b) Asia and (c) Alps. The Asia and Alps domains are shown in Figure 2. Boxplots show the data for 2071–2100 vs. 1981–2010. SSP1-2.6, SSP3-7.0, and SSP5-8.5 are shown in green, brown, and pink colors.

- T_{hmax}: Temperature of the hottest month (in degrees Celsius).
- T_{mmax}: Temperature of the warmest month (in degrees Celsius).
- T_{mmin}: Temperature of the coldest month (in degrees Celsius).
- P_t: Threshold precipitation, calculated as $P_t = 2 \cdot T_a + 14$ for coastal areas and $P_t = 2 \cdot T_a$ for continental areas.

We count the grid points labeled as Tundra and assess the potential shifts in the Köppen Tundra zone.

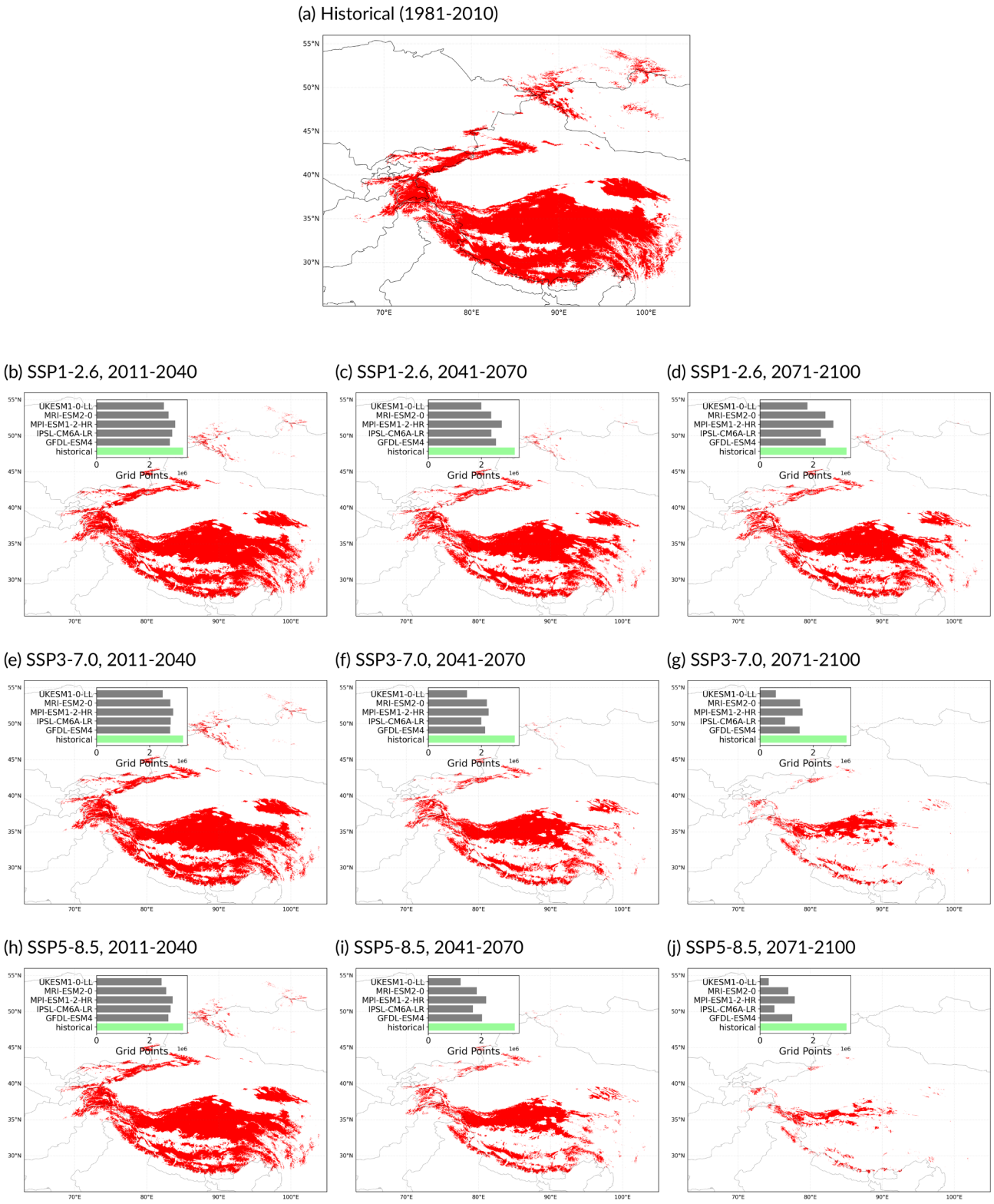

FIGURE 2 Köppen climate classification for the ET (Tundra) climate zone in Asia for a) historical period of 1980–2010 and future scenarios of SSP1-2.6, SSP3-2.6, and SSP5-8.5 (left, middle, and right columns) and for near, middle, and far future (top, middle, and bottom rows). The subfigure in the top left indicates the number of grid points (each representing a 1 k m^2 area) that each model projected for the ET classification. This provides an idea of the extent of agreement among the different models regarding the size of the ET climate zone in the future scenario compared with the historical record. Grid points where all five models agree are only shown in the maps.

3 | RESULTS

3.1 | ISIMIP3b temperature tends

Figure 1 shows a positive warming trend over the next century from the ISIMIP3b climate input dataset on a global scale, as well as over the Asia and the Alps. The boxplots on the right side of Figure 1 illustrate the temperature increase during 2071–2100 compared with the baseline period of 1981–2010.

SSP1-2.6 exhibits the smallest temperature increase across all regions, demonstrating that robust mitigation strategies can significantly avoid future warming. SSP3-7.0 presents less warming than SSP5-8.5. In contrast, SSP5-8.5 reflects the steepest temperature increase toward the end of the century. The data suggest that temperature increases in Asia may exceed the global average, indicating a higher regional sensitivity to global warming. Asia might experience significant warming under all SSP scenarios. Elevated areas are particularly vulnerable to the impacts of climate change (Hock et al., 2019). By the end of the century, the SSP1-2.6 scenario predicts moderate warming, whereas SSP3-7.0 and SSP5-8.5 project more severe temperature increases in the Alps.

3.2 | Tundra climate zone in Asia

Our analysis of the ET (Tundra) climate zone in Asia reveals no significant reduction in this zone during the early part of the century (Figure 2). However, substantial portions of ET might shrink significantly under the SSP3-7.0 and SSP5-8.5 scenarios by mid-century, particularly by the end of the century (more than 60%). The shrinkage of ET seriously threatens water availability in Central Asia (Didovets et al., 2024; Fallah & Rostami, 2024; Flanner et al., 2011). The Tibetan Plateau, functioning as a thermal source, is crucial in influencing the Asian monsoon (Immerzeel et al., 2010; Wu et al., 2012). Diminished snowpack and rising snow lines—a phenomenon associated with "elevation-dependent warming"—can reduce albedo, leading to increased absorption of solar radiation and further amplification of warming (Group, 2015). These changes have the potential to disrupt global atmospheric circulation patterns.

3.3 | Tundra climate zone in Alps

Figure 3 illustrates the potential disappearance of the ET climate class across all scenarios and models by the end of the century. The Tundra zone in the Alps could soon lose half of its coverage under all scenarios. Moreover, by mid-century, two-thirds of the region classified as ET could vanish even under the sustainable SSP1-2.6 scenario, and nearly the entire zone could disappear under SSP3-7.0 and SSP5-8.5. As previously discussed, losing the Tundra climate zone in the Alps could impose severe climatic stress on Europe.

3.4 | Shifts to other climate zones

Due to its permafrost and short growing seasons, the Tundra is typically too cold to support tree growth. However, as temperatures rise, permafrost thaws and the growing season extends, enabling the invasion of boreal forests into Tundra areas. As shown in Figure 4, under the SSP3-7.0 and SSP5-8.5 scenarios, nearly half of the ET zone in Asia is projected to transition to the Dfb (Warm summer continental) climate zone by the end of the century. This shift transforms Tundra regions into climate zones with increased seasonal temperature variability. Such changes are likely to have profound ecological implications, including altered species distributions, changes in water availability, and disruptions to existing ecosystems.

ET zone in Asia might convert significantly to the Dfc (Subarctic, Subalpine) climate classification across all scenarios toward the middle and end of the century. This transformation, coupled with the transition to Dfb, indicates a substantial warming trend that is already affecting the region's climate. The conversion of Tundra areas into subarctic climates suggests that the ecological landscape of Asia will undergo considerable and early changes. These shifts could lead to the expansion of boreal forests into former Tundra regions, potentially disrupting ecosystems, altering hydrological cycles, and impacting biodiversity.

Different than in Asia, in the Alps, the ET climate zone shifts only into Dfb and Dfc categories. The transition from the ET climate classification to Dfb or Dfc in the Alps is particularly dramatic. The complex topography of the Alps directly influences its climate, and warming can cause a significant upward shift in the tree line, leading to a reduction in ET-classified zones. Influenced by Atlantic and Mediterranean weather patterns, the Alps are susceptible to significant climate changes, mainly as snow cover decreases and glaciers retreat due to warming. Figure 5 indicates that by the end of the century, under SSP3-7.0 and SSP5-8.5 scenarios, the ET climate zone in the Alps is expected to transition almost completely to Dfb (25% and 40% for SSP3-7.0 and SSP5-8.5) and Dfc (65% and 55% for SSP3-7.0 and SSP5-8.5) classifications. The transition from ET to

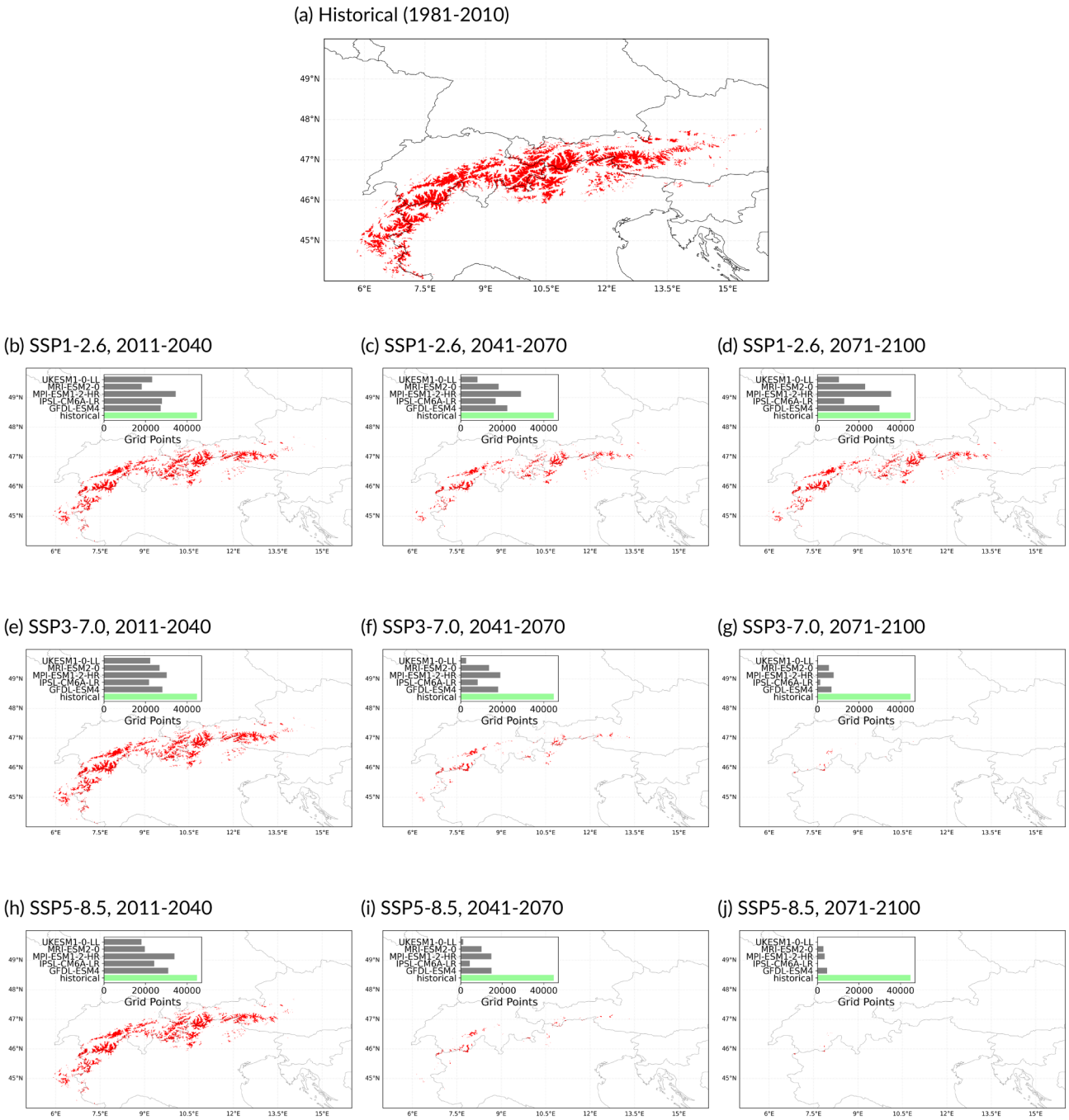

FIGURE 3 As in Figure 2 but for Alps.

Dfc is evident across almost all scenarios and time slices, highlighting the regional warming trend.

4 | DISCUSSION AND CONCLUSION

Our paper contributes to a few studies on climatic zone changes in Asia and the Alps using CMIP6 model outputs (Beck et al., 2018; Thrasher et al., 2022). Using high-resolution Köppen classification, our study reveals a significant reduction in these zones over the Alps and Tibetan Plateau.

The analysis of high-resolution Köppen classifications elucidates ongoing and future shifts within the Tundra climate zones across both the Alps and Asia (answer to the first scientific question Q1). At the end of the century, there might be notable transitions to other climate classifications, such as Dfb and Dfc. The analysis shows that the extent of these shifts is closely

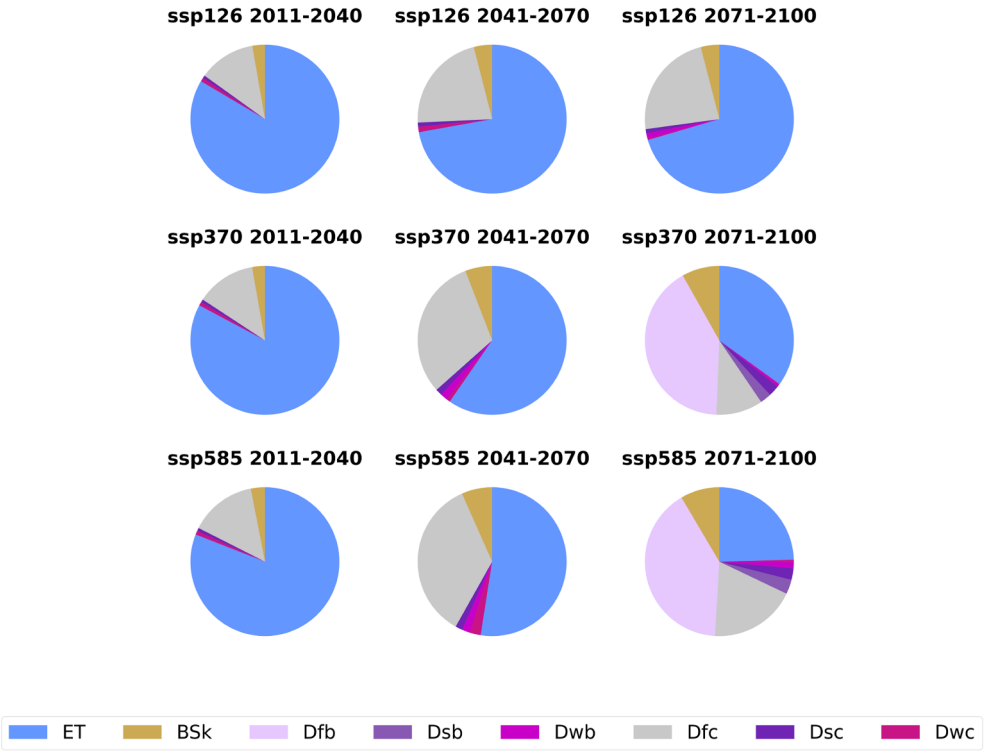

FIGURE 4 Five ISIMIP models' ensemble mean for the migration of Köppen categories from ET during 1981–2010 to other classes for different scenarios and time slices over Asia.

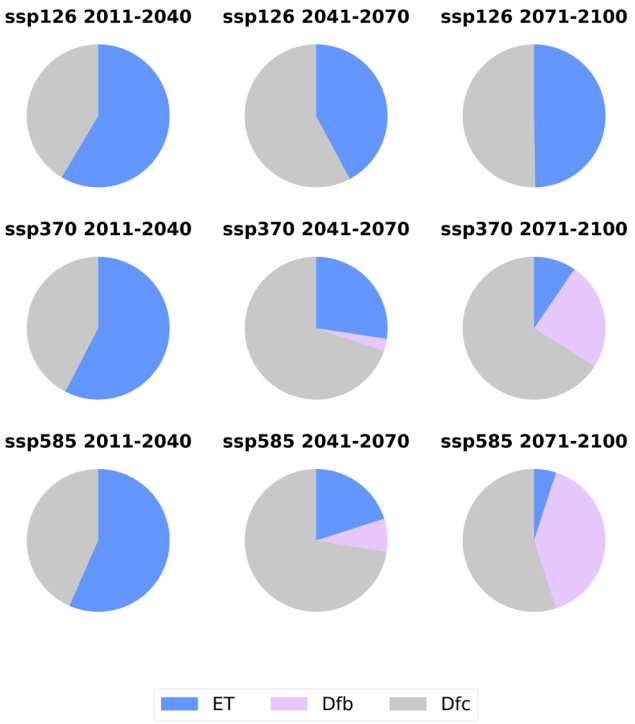

FIGURE 5 As in Figure 4 but over Alps.

linked to the intensity of global warming. The results highlight that these shifts are already underway and are expected to accelerate, particularly in high-altitude regions, where even slight temperature increases can lead to catastrophic outcomes.

We conclude that surpassing a 2°C temperature increase from the 1981–2010 baseline will profoundly impact the geographical distribution and stability of the Tundra climate zone in the Alps and Asia (answer to the second scientific question, Q2). The results indicate that a 2°C temperature rise would likely eliminate the Tundra climate in the Alps and reduce its extent by over 70% in Asia, thereby increasing the significant future risk, particularly in scenarios involving higher greenhouse gas emissions.

Köppen climate classification system provides a valuable framework for categorizing global climate zones. However, it has several caveats: Despite applying bias correction and statistical downscaling, projection uncertainty remains inherent in climate output. By integrating outputs from five structurally independent models with varied climate sensitivities, we embrace a range of possible futures, thereby incorporating inherent uncertainty into our results. Our approach does not claim high precision in future projections but seeks to provide fair possible estimates given the current state of climate science.

Increasing the number of simulations may enlarge the sample size of potential future climate states. Another approach would be to include dynamically downscaled models. However, there are still very few such simulations for Asia, especially the ones driven by CMIP6 models. That could help address some model uncertainties that statistical downscaling methods may not capture. It is also essential to consider the limitations of

statistical methods, including issues related to stationarity and the fact that such approaches need high-quality gridded observational datasets. Such datasets might be available for the Alps, but Asia still has a massive gap.

AUTHOR CONTRIBUTIONS

Bijan Fallah: Methodology (equal); writing – original draft (equal). **Masoud Rostami:** Conceptualization (supporting); formal analysis (supporting); investigation (supporting); methodology (supporting); writing – original draft (supporting). **Iulii Didovets:** Conceptualization (supporting); formal analysis (supporting); methodology (supporting); validation (supporting); writing – original draft (supporting). **Zhiwen Dong:** Writing – original draft (supporting).

ACKNOWLEDGMENT

Open Access funding enabled and organized by Projekt DEAL.

FUNDING INFORMATION

This project is funded by the German Foreign Office as part of the Green Central Asia project and Virgin Unite USA, Inc. in collaboration with the Planetary Boundary Science Lab project.

CONFLICT OF INTEREST STATEMENT

The authors report no conflict of interest.

DATA AVAILABILITY STATEMENT

This paper's Python code for analysis is available at https://zenodo.org/records/10635817 with DOI: 10.5281/zenodo.10635816. For the code used to produce Figure 1, please contact Christoph Menz (https://www.pik-potsdam.de/members/menz). For data availability, please refer to the data and Methods section of the manuscript.

ORCID

Bijan Fallah https://orcid.org/0000-0003-3302-2030
Masoud Rostami https://orcid.org/0000-0003-1730-5145

REFERENCES

Beck, H.E., Zimmermann, N.E., McVicar, T.R., Vergopolan, N., Berg, A. & Wood, E.F. (2018) Present and future köppen-geiger climate classification maps at 1-km resolution. *Scientific Data*, 5, 1–12.

Brown, C., Brown, E., Murray-Rust, D., Cojocaru, G., Savin, C. & Rounsevell, M. (2015) Analysing uncertainties in climate change impact assessment across sectors and scenarios. *Climatic Change*, 128, 293–306.

Clima, T. & Te, W. (2023) *State of the climate in Asia*. Geneva: WMO.

Dee, D.P., Uppala, S.M., Simmons, A.J., Berrisford, P., Poli, P., Kobayashi, S. et al. (2011) The era-interim reanalysis: configuration and performance of the data assimilation system. *Quarterly Journal of the Royal Meteorological Society*, 137, 553–597.

Didovets, I., Krysanova, V., Nurbatsina, A., Fallah, B., Krylova, V., Saparova, A. et al. (2024) Attribution of current trends in streamflow to climate change for 12 central asian catchments. *Climatic Change*, 177, 16.

Dunford, R., Harrison, P. & Rounsevell, M. (2015) Exploring scenario and model uncertainty in cross-sectoral integrated assessment approaches to climate change impacts. *Climatic Change*, 132, 417–432.

Dunford, R.W., Smith, A.C., Harrison, P.A. & Hanganu, D. (2015) Ecosystem service provision in a changing europe: adapting to the impacts of combined climate and socio-economic change. *Landscape Ecology*, 30, 443–461.

Eyring, V., Bony, S., Meehl, G.A., Senior, C.A., Stevens, B., Stouffer, R.J. et al. (2016) Overview of the coupled model intercomparison project phase 6 (cmip6) experimental design and organization. *Geoscientific Model Development*, 9, 1937–1958.

Fallah, B., Cubasch, U., Prömmel, K. & Sodoudi, S. (2016) A numerical model study on the behaviour of asian summer monsoon and amoc due to orographic forcing of tibetan plateau. *Climate Dynamics*, 47, 1485–1495.

Fallah, B. & Rostami, M. (2024) Exploring the impact of the recent global warming on extreme weather events in central asia using the counterfactual climate data attrici v1. 1. *Climatic Change*, 177, 80.

Fallah, B., Russo, E., Menz, C., Hoffmann, P., Didovets, I. & Hattermann, F.F. (2023) Anthropogenic influence on extreme temperature and precipitation in central asia. *Scientific Reports*, 13, 6854.

Flanner, M.G., Shell, K.M., Barlage, M., Perovich, D.K. & Tschudi, M. (2011) Radiative forcing and albedo feedback from the northern hemisphere cryosphere between 1979 and 2008. *Nature Geoscience*, 4, 151–155.

Flato, G., Marotzke, J., Abiodun, B., Braconnot, P., Chou, S.C., Collins, W. et al. (2014) Evaluation of climate models. In: *Climate change 2013: the physical science basis. Contribution of working group I to the fifth assessment report of the intergovernmental panel on climate change*. Cambridge, UK, and New York, NY: Cambridge University Press, pp. 741–866.

Geiger, A., Lenz, P. & Urtasun, R. (2012) Are we ready for autonomous driving? The kitti vision benchmark suite. In: *IEEE conference on computer vision and pattern recognition (CVPR) 2012*. New York, NY: IEEE, pp. 3354–3361.

Group, M. R. I. E. W. (2015) Elevation-dependent warming in mountain regions of the world. *Nature Climate Change*, 5, 424–430.

Hock, R., Rasul, G., Adler, C., Cáceres, B., Gruber, S., Hirabayashi, Y. et al. (2019) High mountain areas. In: *IPCC special report on the ocean and cryosphere in a changing climate*, Cambridge: Cambridge University Press, pp. 131–202.

Holman, I. & Cojocaru, G. (2011) Report describing the integrated assessment platform (iap) specification, meta-model specifications and the multi-scale approach. climsave deliverable 2.1.

Immerzeel, W.W., Van Beek, L.P. & Bierkens, M.F. (2010) Climate change will affect the asian water towers. *Science*, 328, 1382–1385.

Jäger, J., Rounsevell, M., Harrison, P., Omann, I., Dunford, R., Kammerlander, M. et al. (2015) Assessing policy robustness of

climate change adaptation measures across sectors and scenarios. *Climatic Change*, 128, 395–407.

Karger, D.N., Conrad, O., Böhner, J., Kawohl, T., Kreft, H., Soria-Auza, R.W. et al. (2017) Climatologies at high resolution for the earth's land surface areas. *Scientific Data*, 4, 1–20.

Karger, D.N., Schmatz, D.R., Dettling, G. & Zimmermann, N.E. (2020) High-resolution monthly precipitation and temperature time series from 2006 to 2100. *Scientific Data*, 7, 248.

Karger, D.N., Wilson, A.M., Mahony, C., Zimmermann, N.E. & Jetz, W. (2021) Global daily 1 km land surface precipitation based on cloud cover-informed downscaling. *Scientific Data*, 8, 307.

Kebede, A., Dunford, R., Audsley, E., Harrison, P., Holman, I., Mokrech, M. et al. (2015) The sensitivity of cross-sectoral impacts to climate and socio-economic drivers for key european sectors. *Climatic Change*, 128, 261–277.

Lange, S. (2019) Trend-preserving bias adjustment and statistical downscaling with isimip3basd (v1. 0). *Geoscientific Model Development*, 12, 3055–3070.

Lange, S. (2021) Isimip3 bias adjustment fact sheet. Technical Report.

Lange, S., Menz, C., Gleixner, S., Cucchi, M., Weedon, G.P., Amici, A. et al. (2021) *Wfde5 over land merged with era5 over the ocean (w5e5 v2. 0)*. Potsdam: ISIMIP.

Lawrimore, J.H., Menne, M.J., Gleason, B.E., Williams, C.N., Wuertz, D.B., Vose, R.S. et al. (2011) An overview of the global historical climatology network monthly mean temperature data set, version 3. *Journal of Geophysical Research: Atmospheres*, Washington, DC: American Geophysical Union (AGU), 116.

O'neill, B., Tebaldi, C., Van Vuuren, D., Eyring, V., Friedlingstein, P., Hurtt, G. et al. (2016) The scenario model intercomparison project (scenariomip) for cmip6. *Geoscientific Model Development*, 9, 3461–3482.

Peel, M.C., Finlayson, B.L. & McMahon, T.A. (2007) Updated world map of the köppen-geiger climate classification. *Hydrology and Earth System Sciences*, 11, 1633–1644.

Schneider, U., Becker, A., Finger, P., Meyer-Christoffer, A., Rudolf, B. & Ziese, M. (2014) Gpcc's new land surface precipitation climatology based on quality-controlled in situ data and its role in quantifying the global water cycle. *Theoretical and Applied Climatology*, 115, 15–40.

Song, J.-H., Kang, H.-S., Byun, Y.-H. & Hong, S.-Y. (2010) Effects of the tibetan plateau on the asian summer monsoon: a numerical case study using a regional climate model. *International Journal of Climatology: A Journal of the Royal Meteorological Society*, 30, 743–759.

Thrasher, B., Wang, W., Michaelis, A., Melton, F., Lee, T. & Nemani, R. (2022) Nasa global daily downscaled projections, cmip6. *Scientific Data*, 9, 262.

Wu, G., Liu, Y., He, B., Bao, Q., Duan, A. & Jin, F.-F. (2012) Thermal controls on the asian summer monsoon. *Scientific Reports*, 2, 404.

How to cite this article: Fallah, B., Rostami, M., Didovets, I., & Dong, Z. (2024). High-resolution CMIP6 analysis highlights emerging climate challenges in alpine and Tibetan Tundra zones. *Meteorological Applications*, *31*(5), e70001. https://doi.org/10.1002/met.70001